


Article

Fracture Network Analysis of Karstified Subis Limestone Build-Up in Niah, Sarawak

Poh Yee Ong^{1,2,*} and Siti Nur Fathiyah Jamaludin^{1,3} 

¹ Department of Geosciences, Universiti Teknologi PETRONAS, Seri Iskandar 32610, Malaysia; fathiyah.jamaludin@utp.edu.my

² Centre for Subsurface Imaging, Institute of Hydrocarbon Recovery, Universiti Teknologi PETRONAS, Seri Iskandar 32610, Malaysia

³ South East Asia Carbonate Research Laboratory, Institute of Hydrocarbon Recovery, Universiti Teknologi PETRONAS, Seri Iskandar 32610, Malaysia

* Correspondence: pohyee.ong0517@gmail.com or poh_22004613@utp.edu.my

Featured Application: Geological carbon storage site.

Abstract: Understanding complex carbonate fracture networks and karstification at various geological scales is challenging, especially with limited multi-scale datasets. This paper aims to reduce uncertainty in the fracture architecture of Central Luconia karstified reservoirs by narrowing observational gaps between seismic and well data by using the discrete fracture models of exposed limestone outcrops as analogues for the subsurface carbonate reservoir. An outcrop-based fracture network characterisation of a near-surface paleo-karst at Subis Limestone combined with lineament analysis was conducted to extract fracture parameters. The karst structure was first delineated using a digital elevation map and outcrop examination. Then, topology analysis was performed, following the creation of two-dimensional discrete fracture models. Two main fracture sets oriented northeast–southwest and northwest–southeast and 79 potential dolines were identified. Fracture intersections, northeast–southwest major orientations, and drainage systems highly influenced the karst features. The Subis Limestone fracture model revealed that the highest number of fractures and total length of fractures were concentrated in the northern part of the Subis Limestone build-up (X: 250–350, Y: 150–250) and became denser towards the northwest direction of the outcrop (X: 600–800). The fractures in the Subis paleo-karsts appear isolated, with I-nodes ranging from 0.74 to 0.94. Hence, it is crucial to incorporate matrix porosity into multiple scales of fracture network modelling to improve upscaling and the modelling of fracture–vug networks, as well as to minimise the underestimation of discrete fracture networks in fractured and karstified limestone.

Keywords: fractured carbonate reservoirs; outcrop analogue; discrete fracture network; fractures; karst; topology; Subis limestone



Citation: Ong, P.Y.; Jamaludin, S.N.F. Fracture Network Analysis of Karstified Subis Limestone Build-Up in Niah, Sarawak. *Appl. Sci.* **2023**, *13*, 12110. <https://doi.org/10.3390/app132212110>

Academic Editor: Sotirios Kokkalas

Received: 21 August 2023

Revised: 13 October 2023

Accepted: 14 October 2023

Published: 7 November 2023



Copyright: © 2023 by the authors. Licensee MDPI, Basel, Switzerland. This article is an open access article distributed under the terms and conditions of the Creative Commons Attribution (CC BY) license (<https://creativecommons.org/licenses/by/4.0/>).

1. Introduction

Naturally fractured carbonate reservoirs are characterised by complex internal architecture due to diagenesis, karstification, and faulting processes. The Miocene carbonate reservoirs in Central Luconia Province, Sarawak, located in northwest Borneo Island, are mainly affected by syn-rift- or post-rift-induced faults and fractures [1]. The intensity and distribution of the fractures significantly impact the evaluation of these carbonate reservoirs as potential sites for carbon storage [2,3]. The substantial secondary porosity in the carbonates is proposed as an option for the security of the long-term storage of carbon dioxide [4–7]. In carbonates, the geometry, attitude, and distribution of fault-related fractures and subsidiary faults can significantly influence the genesis and evolution of karst features [8]. Fractures affect the porosity and permeability properties because they

are prone to karstification, which induces permeability and porosity [9] while providing preferential paths for fluid circulation and potential storage capacity in fractured reservoirs.

Estimating storage and flow requires fracture network modelling with matrix and karst porosity considerations. This could eliminate uncertainty in appraising potential carbon storage sites in carbonate reservoirs. The term “carbon” in this paper refers to “carbon dioxide”. However, due to the existence of a vuggy system that produces intricate matrix–fracture interactions in carbonate reservoirs, simulating a reasonable fracture network and its connectivity in naturally fractured carbonate reservoirs remains a challenge for researchers [9–12]. Other issues include the magnitude and resolution of the fractures applied in the modelling. Due to the limited dataset, only specific sizes or scales of fractures could be modelled, which is common, especially in the sub-seismic fracture networks [13–16]. Ideally, to properly depict the fracture network within a carbonate platform reservoir, a comprehensive dataset with a resolution ranging from micro-scale to macro-scale is required; however, capturing all the data at once is ambitious and challenging.

Three-dimensional (3D) seismic data are commonly employed in the industry as the primary source for subsurface structural interpretation at scales from several kilometres to a few meters [17–19]. However, faults and fractures below the seismic volume resolution are often excluded from the interpretation and are referred to as sub-seismic. They typically measure less than 25 m and are only detected through borehole [17–21] and core data.

An analogue outcrop study is incorporated into the fracture network modelling approach to bridge the observational gap between well and seismic data. Due to changes in stratigraphy, facies, uplift history, and associated stress release during the post-uplift event, the statistical structural analysis performed on outcrop analogues cannot directly apply to deep subsurface prediction. However, analysing the analogue may lead to a better understanding of the subsurface condition and reduce ambiguity at the fracture scale. Analogue studies allow for a detailed structural characterisation of fracture networks at several scales, spanning from millimetres to metres and providing a better solution for upscaling in modelling the fracture network and reducing fracture underestimation [13,15,22,23]. Furthermore, a better prediction of the subsurface can be formed by considering the impact and origin of secondary porosity and permeability.

In summary, this study detailed the outcrop-based characterisation of a near-surface carbonate karst system in the Niah National Park, Sarawak, Malaysia. The study focused on the relationship between fractures and paleo-karst features, using an analogue from the Niah Cave-Subis Limestone complex acquired through field and digital structural analyses. The analogue study aimed to provide valid qualitative descriptions to support the quantitative characterisation of fractures at the macro- and meso-scale. This work also demonstrated the significance of characterising sub-seismic-scale fractures in modelling the connectivity of karstified carbonate reservoirs and their impact on karstification.

2. Study Area and Geological Settings

2.1. Study Area

The Subis build-up is a massive, cliff-forming coralline limestone hill that hosts the famous Niah Great Cave at the northern flank of the build-up (Figure 1). It is located northwest of the Tinjar Province and extends over 30 km², with a peak elevation of 394 m. The northeast–southwest-trending Trusan Fault slices through the build-up and divides it into two major blocks. The Great Cave and Painted Cave towers are the most accessible Subis build-up towers. The Great Cave (Figure 1e) is complex, with several wide passages and high chambers with ceiling openings, while the Painted Cave is located southeast of the limestone complex [24]. The Subis Limestone is commonly used as an analogue for Central Luconia carbonates. Previous studies on the Subis Limestone have focused on the biostratigraphy and sedimentology of carbonate rocks [25–29] and speleology [24,30–32] with no mention of the fracturation history of the outcrop.

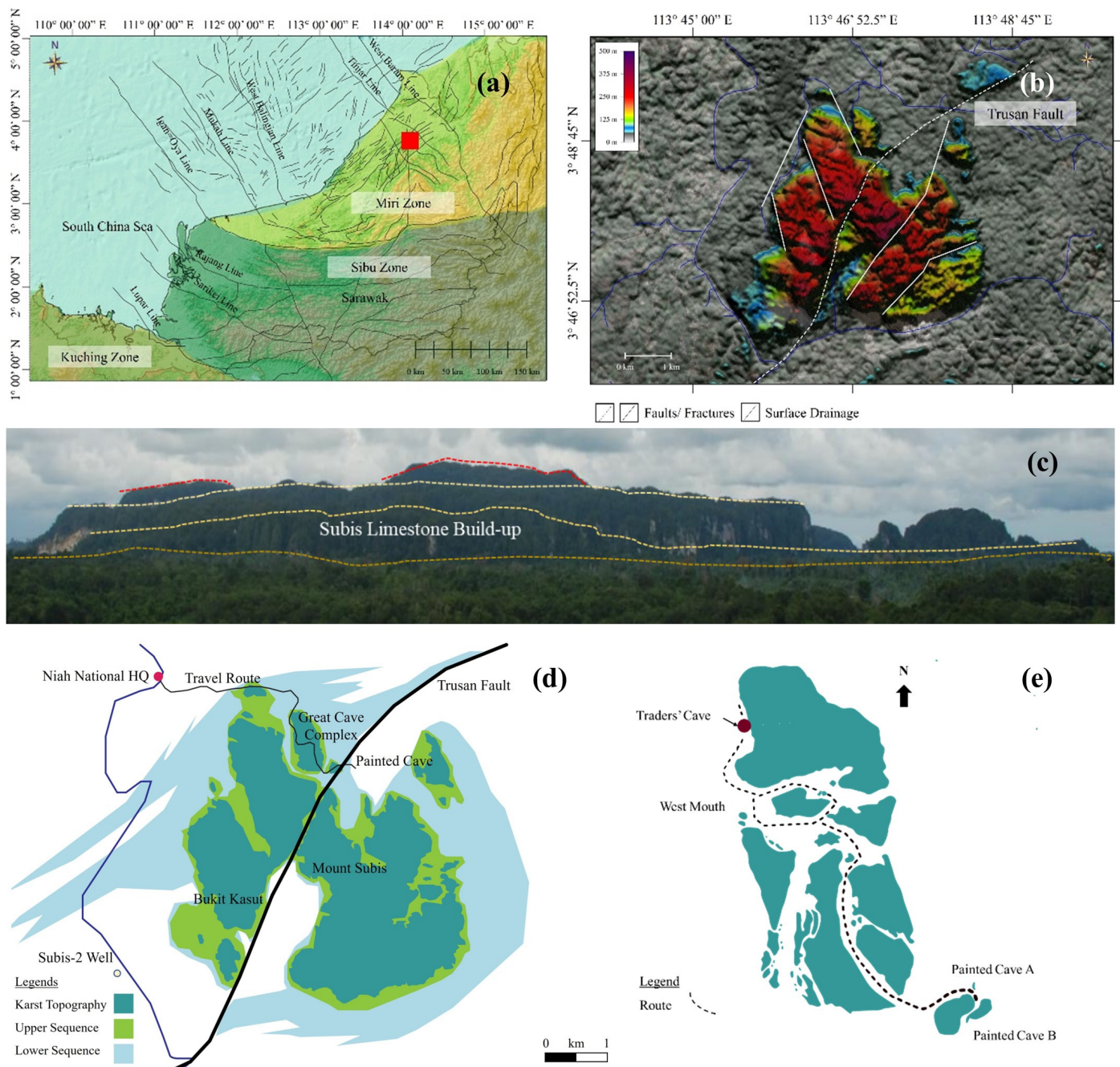


Figure 1. (a) Location map of the study area, Subis Limestone, in Niah, Sarawak (red square), with emphasis on the tectonic features [1,33–36]. (b) Subis build-up on SRTM-Digital Elevation Model (DEM) overlay with a satellite image for clearer lineament delineation. The Subis build-up was divided into two sections by an NE–SW-trending Trusan Fault (white solid line) with several identified internal faults (white dotted lines) that separate the mega limestone into isolated build-ups. (c) Flat-top geomorphology of Subis Limestone with the upper portion of the catch-up phase. Different elevations of vegetation indicate the third-order sequence boundary due to sea level changes, now represented by three horizons (base-, inter-, and top-carbonate layers). (d) Karst topography distribution [29]. The route of the fieldwork began from the Niah National Park headquarters (HQ) to the Painted Cave. (e) A detailed route map within the Great Cave Complex and Painted Cave. The karst features and fault/ fracture evidence were observed along this route.

2.2. Tectonic Evolution

Borneo Island, which hosts the Niah–Subis Limestone, originated from a group of micro-continental fragments [37–39]. The Sarawak Basin is a fore-deep basin located at the eastern end of the Sundaland shelf, commonly known as northwest of Borneo Island. Although Borneo Island is currently geologically stable, it has, historically, been subjected to intense tectonic activity that altered the architecture of the carbonate build-ups [36,40,41].

The western interior zone of Borneo's basement comprises Palaeozoic and Mesozoic igneous, sedimentary, and metamorphic rocks that acted as a craton during the Middle to Late Tertiary [37]. During the Paleocene, the Luconia Block drifted away from China and towards Borneo [39,42], and the floor between Borneo and the Luconia Block was subducted beneath Borneo. Subduction occurred along the Lupar Line, which extended into central Kalimantan, resulting in an accretionary complex comprised of the Rajang Group rocks, which formed the mountain range in central Borneo. The subduction aided the transition from a deep marine setting in the Sarawak Basin to a shallower environment to the southwest, allowing coral reefs to thrive [43]. During the Middle Miocene, the Luconia Block collided with the crust of central Borneo. This impact further elevated the Rajang Mountain Range in central Borneo [33]. Borneo experienced regional uplift after the Middle Miocene, resulting in massive deltaic systems that overlie the older marine deposits in Sarawak, thereby terminating carbonate sedimentation [44]. During the Pliocene, Sarawak underwent compressional deformation, which was most likely caused by (1) the subduction of the Proto-South China Sea (PSCS) through the North Borneo Trough or (2) by transpression along strike-slip faults generated by the extrusion of the Indo-China Block across the South China Sea up to Sarawak [45].

The main tectonic domains of the study area are the Miri, Sibiu, and Kuching Zones, which represent the North, Central, and Southwest of Sarawak, respectively [25,33,46,47]. The Miri Zone, limited to the south by the Bukit Mersing Line (BML) and to the north by the Jerudong Fault [48], is where the Niah–Subis Limestone complex was formed. The Miri Zone comprises less deformed shallow marine and deltaic siliciclastic rocks that overlie the Oligocene–Miocene deltaic to marine sediments (Tatau, Nyalau, Setap Miri, and Lambir and Tukau formations). These sediments are predominantly clastics with some isolated carbonate build-ups (Melinau, Subis, Suai, and their equivalent limestones).

Large swathes of the Sarawak terrain are characterised by an arcuate fold and thrust belt, also known as the northwest Borneo Rajang Group fold–thrust belt, which extends over 1000 km along the strike and has a width of more than 300 km [33,34]. Meanwhile, the structural trend lines run in broad curves in central and north Sarawak. Tight, overturned folds are common within these zones and are interrupted by a series of thrust faults. Following the fold–thrust event in central Sarawak, strike-slip reactivation of pre-existing faults occurred. Northwest–southeast compression or left-lateral strike-slip motion along North–northwest-trending faults has resulted in folds as well as normal, strike-slip, and thrust faults [34]. The Tinjar Line is a northeast to north–northeast-trending dextral transform fault that accommodated the spreading and subduction of the Proto-South China Sea beneath northwest Borneo from the Eocene to Early Miocene [49–51].

2.3. Depositional Setting and Stratigraphy

The Subis Limestone was deposited during the Early Miocene [29,52] and is equivalent to Cycle II limestone (Late Oligocene to Early Miocene) [25,27,29,33]. It is massively bedded, homogenous, and comprises algal–coral reefal facies with no interbedded mudstones deposited in a calm, clear-water, shallow inner-sea setting with normal salinity [25]. The intense vegetation and biochemical activity in Sarawak's tropical setting have favoured karst formation, increased water acidity, and enhanced karst development and weathering features. Karstification occurred in five identified phases from the Pleistocene period to recently due to repeated fluctuations in uplift and eustatic sea level changes, which eventually culminated in the burial of the build-up by excessive clastic sediment influx [27].

Subis Limestone is a member of the Tangap Formation, which is flanked by the Setap Shale Formation and interfingers with the sand-rich Nyalau Formation [33]. The Upper Batu Gading and Upper Melinau Limestones to the east and the west of the Subis Limestone are the most prominent Early Miocene carbonates that can be correlated to the Subis Limestone. Meanwhile, shelf-edge carbonates that mark the open margin area have been reported further to the northeast [53].

3. Materials and Methods

Transdisciplinary and multi-scale fracture network characterisation was performed utilising digital satellite imagery, drainage patterns, and geological scrutinization acquired during the fieldwork on the Niah–Subis Limestone. First, the structural geological investigations of the linear features were examined, marked, and recorded on the Digital Elevation Model (DEM). The linear features of the DEM represent geological lineaments, which range from fractures, faults, folds, sedimentary bedding, and possible lithological boundaries. The present-day Niah–Subis drainage pattern map helped the lineament delineation of the DEM to enhance the patterns for lineament interpretation. The potential karst depression at the regional scale was identified using DEM, and the relationship between the karst depression and the surface drainage system was then evaluated. Fieldwork was conducted in Traders’ Cave, Great Cave, and Painted Cave with visible observation for the Subis Limestone outcrops. During the fieldwork, a close geological examination was performed to differentiate karst features and fractures in the outcrops. Measurements of the fracture orientations were recorded for comparison with the lineament analysis conducted on the DEM data. Lastly, the network topology analysis is combined with the two-dimensional (2D) discrete fracture (DFN) modelling of the regional lineaments and outcrop-scale fractures. The discrete fracture network (DFN) model comprises a series of geometric objects representing individual fractures [54]. When integrated, the network topology emphasises the relationships between individual structures and can reveal how fault interactions and connectivity occur [55,56]. The summary of the workflow is displayed in Figure 2.

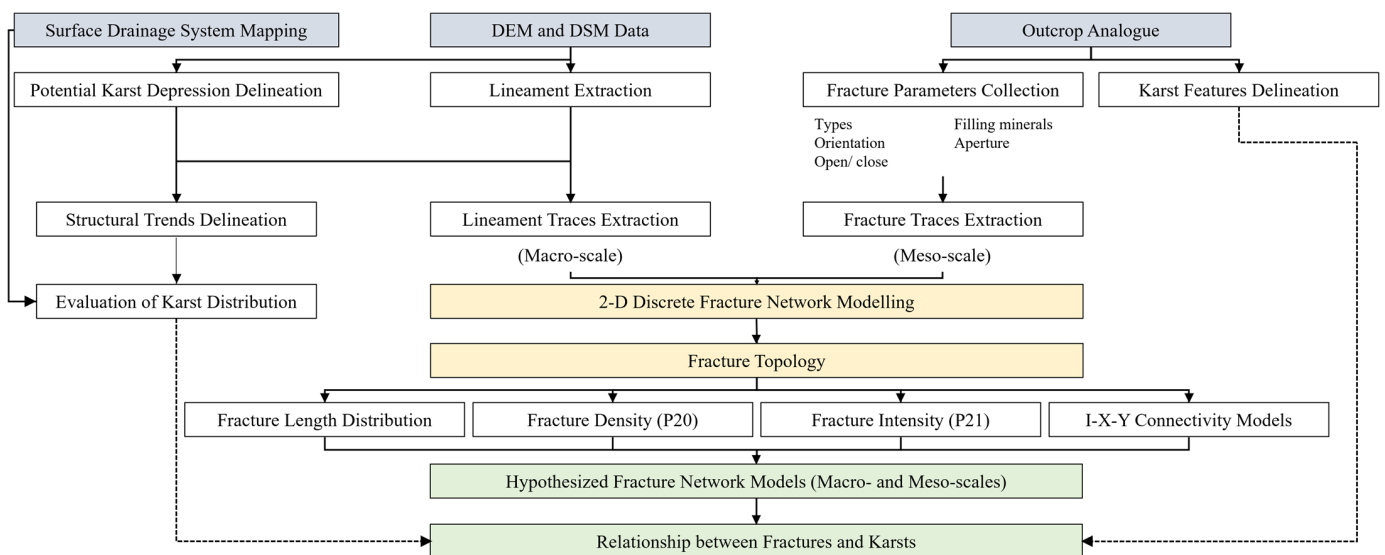


Figure 2. Summary of the workflow for the fracture network analysis of karstified carbonate build-up.

3.1. Structural Studies

3.1.1. Lineament Analysis

Lineament analysis was performed on both the Digital Elevation Model (DEM, SRTM-1 Arc-Second Global) downloaded from [57] and the Digital Surface Model (DSM, ALOS World 3D—30 m) downloaded from [58], with a resolution of approximately 30 m. The density, length, and orientation of the lineaments were analysed. The low resolution of the DEM and DSM images in the low-relief Niah Cave area covered by intense vegetation may

have caused an underestimation of the structural investigations. As such, the lineament analysis between the DEM and DSM was compared with the aid of satellite imagery and topographic maps for regional feature identification to enhance the visualisation of the lineaments while lineament extraction was performed manually.

Lineaments are natural, rectilinear surface features that can be identified as faults, discontinuities, or weakness zones. The shader was generated using the software Global Mapper from the DEM and DSM images, which were then visually checked for lineament delineation. To avoid misinterpretation, several illustrative azimuths of the shader maps were compared, and the lineaments were utilised to calculate the fracture density (number of fractures per unit area), P20, and intensity (total length of fractures per unit area), P21.

3.1.2. Surface Drainage System Mapping

The drainage system is critical in the development and evolution of the karst features. Water–rock interactions will either enlarge the fractures via dissolution or seal the fracture aperture through precipitation. As a result, the fracture network complexity in the karstified carbonate is influenced. Hence, the surface drainage in the Niah River Basin was mapped using [59] and satellite images to establish the interaction between the Niah–Subis Limestone build-up and the surrounding drainage system. The map of the drainage system is shown in Figure 3.

3.1.3. Outcrop Analysis

Outcrops along the walking trails of the Niah National Park, from the entrance towards the Niah Cave, were selected for the structural analysis of the fracture. As the Niah Cave is a National Park, visitors were not permitted to leave the walking pathways. As a result, the data collection was limited to outcrops that were accessible and visible along the designated pathways and staircases. Visible fractures were evaluated and digitised to compute the fracture topology and characterise the connectivity of the fracture network. Any discontinuities were identified as fractures in this study. Fracture characteristics such as fracture type, size, filling (close or open), infill minerals, and aperture were studied during the outcrop visit.

3.2. Karst Features Delineation

Apart from identifying fractures and faults in the field, karst features such as caves, dolines/sinkholes, karst depressions, and speleothems were found and examined. Sinkholes or dolines are the most common karst features [60]. A DEM combined with a topographical map delineated the karst depression [60,61]. As one of the prevalent features of karstification, closed depressions were categorised as potential (future) karst depressions. However, the coarse resolution of the DEM in the study area was insufficient to distinguish fine-scale karst features (less than several metres). On the other hand, ALOS-DSM could identify larger sinkholes indicated by SRTM-DEM. Thus, SRTM-DEM and ALOS-DSM data may be used for the large-scale mapping of karst features in the Subis Limestone, ranging from metres to kilometres.

3.3. Discrete Fracture Network (DFN) Modelling

This study mapped fracture patterns based on the DEMs and exposed outcrops. The geologically mapped fracture networks were then used to investigate the fracture formation process and determine fracture distribution statistics and scaling. Two-dimensional (2D) discrete fracture models were generated from the Niah's regional lineaments and limestone outcrops in the northern area of the Subis build-up. The traced DFNs were then utilised to quantitatively model the fracture distribution using FracPaQ, an open-source MATLAB toolbox [62].

The topology of lineament and outcrop-scale fracture networks was investigated thoroughly. Topology is a tool that allows for the proper characterisation of the connectivity and relationships between fractures [14,63]. In this part, the I–X–Y model is applied to

characterise the dominant control for the fracture network. Manocchi [63] devised the I–X–Y model, which is a ternary plot for the interconnectivity of a fracture network based on scanlines. It depicts the relative proportions of isolated (I), splay or abutment (Y), and intersecting (X) nodes in the fracture network (Figure 4). A better-connected fracture pattern plots closer to the triangle’s base, where there is a higher fraction of X + Y nodes (Figure 5).

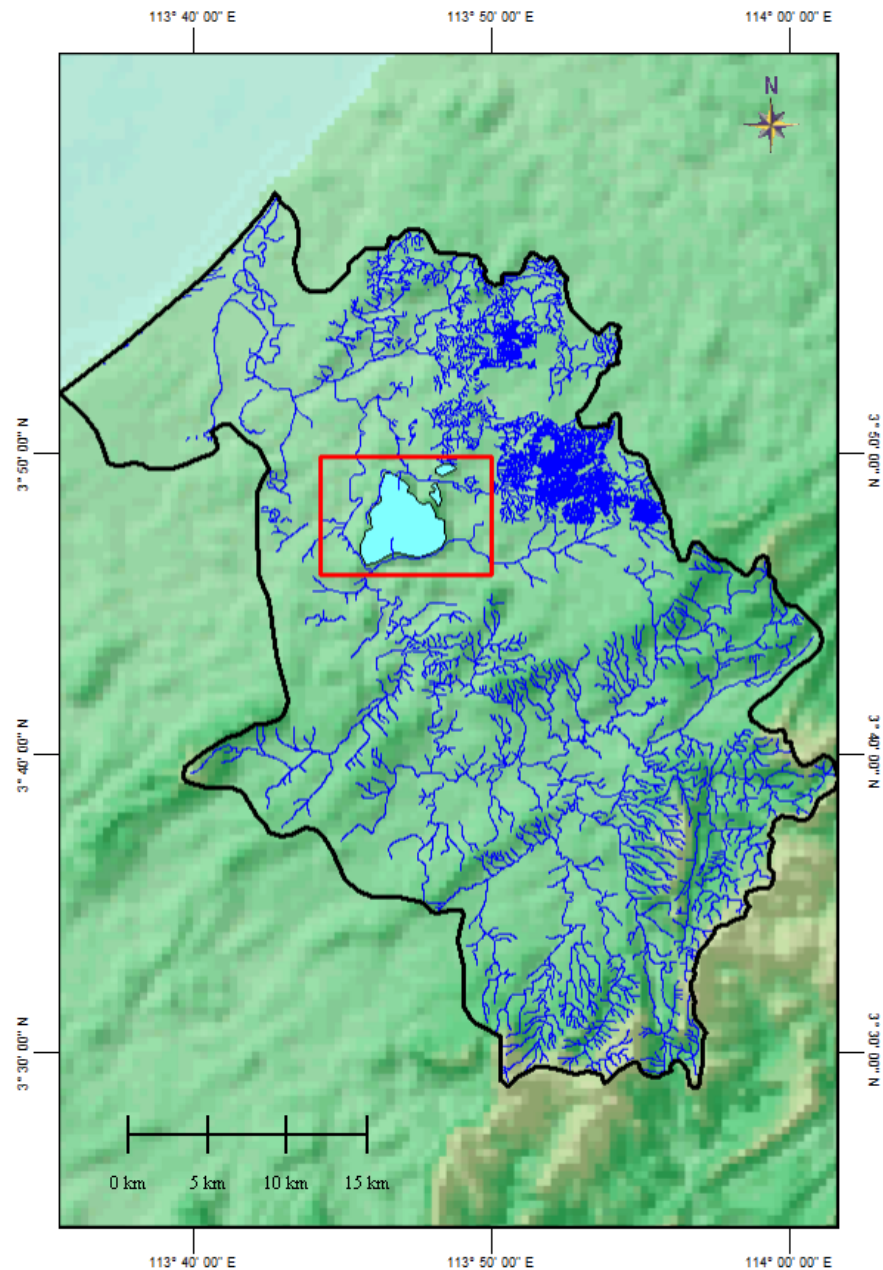


Figure 3. Surface drainage system bounded by the Niah River Basin (Official Website of Department of Irrigation and Drainage Sarawak). The density of the drainage decreases when closer to the Niah–Subis Limestone (light blue).

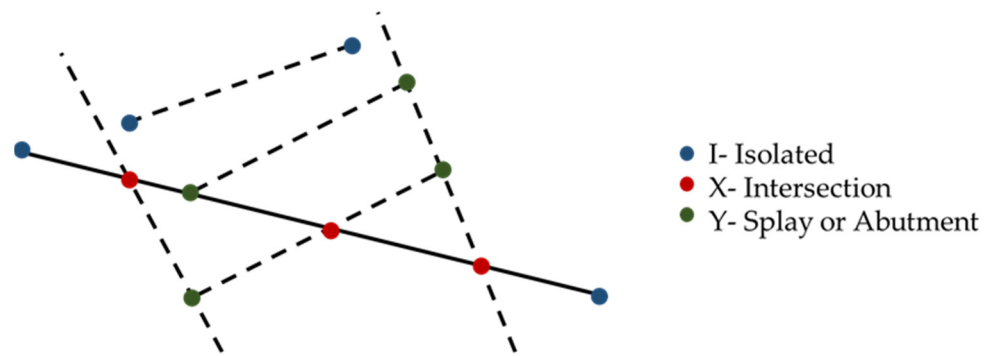


Figure 4. Fracture trace (solid line) with associated crossing fractures (dashed lines), defining the network topology in fracture sets using isolated (I), intersection (X), and splay (Y) nodes.

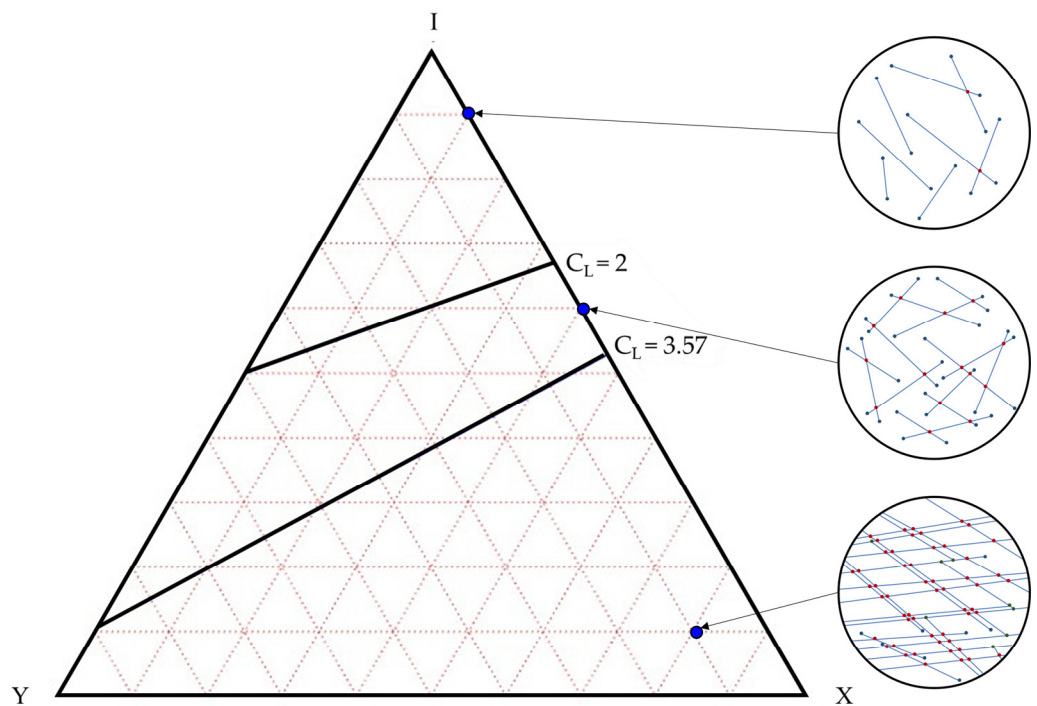


Figure 5. Triangular plot of I–X–Y proportion, based on Manzocchi [63]. C_L (contour line) represents the average number of connections per line (black solid lines). The specific values of intersections per line were described by Sanderson and Nixon [56]. The three sets of traces that simulate fracture networks show how the fracture network topology is characterised using the I–X–Y parameters.

4. Results

4.1. General Morphology of the Study Area

The Niah–Subis Limestone complex, as an onshore paleo-karst outcrop analogue in North Sarawak, displays distinct morphological and geometrical traits. The structure of the Niah–Subis Limestone complex suggests that the carbonate build-up occurred on a paleo-structural high formed by the Nyalau sand shoals of the Tangap Formation, as evidenced by the complex’s exceptional elevations above the surrounding terrain. The limestone build-up has various horizons (i.e., base-, inter-, and top-carbonate layers) (Figure 1c). According to the eustatic sea-level curve obtained by Haq et al. [64], the elevations (represented by the base-, inter-, and top-carbonate layers) were recognised as a major break of a third-order sequence boundary that occurred during the Early Miocene sea-level decline. The morphology, architecture, facies, depositional sequence, and model of the Subis Limestone were identical to those of the offshore Central Luconia carbonate build-ups (Table 1).

Table 1. Properties of the Subis Limestone build-ups as an analogue for offshore Central Luconia carbonates [24,27,29].

Properties	Subis Limestone
Age of host limestone	Late of Oligocene to Early Miocene
Age of karst development	Pleistocene to recent
Influence by sea-level fluctuations	Yes (third order sequence)
Influence by tectonic (uplifting)	Yes
Host lithology	Coralline limestone
Morphology and geometry	Flat-top and layer cake architecture
Dominant foraminifera	Massive/branching corals, benthic foraminifera, and algae
Depositional environment	Quiet, clean-water, shallow inner-sea setting under normal salinity

The Traders' Cave and the Great Cave Complex of the Subis Limestone build-up have their entrances on a west-facing cliff of a steep-sided karst tower located in the northwest of the entire Subis build-up (Figure 1d,e). The Traders' Cave is a vast isolated passage that extends mainly north–south and parallel to the cliff. In contrast, the Great Cave Complex comprises intricate passages that mostly trend in the east–west and north–south directions. The cave entrances are estimated to be 80 m tall, with the overall karst hill standing between 180 m and 190 m tall. Conjugate fractures encircle the karst hill on all sides. The Traders' Cave's exit leads to the Great Cave's entrance via the timber walkway in the south and is connected to the route to the Painted Cave in the southeast. The passages form laterally extensive networks that consist of massive karst passages.

According to the recent surface drainage network of the Niah River basin (Figure 2), the intensity of surface drainage decreased as it reached the Subis paleo-karst build-up. This suggests that the surface water had permeated the underground karstic system and thus cannot be observed from the plan view. Small streams can be observed along the timber walkway and in the Traders' Cave. Therefore, the paleo-karst geomorphology was generated by the dissolution and precipitation reaction of both surface and ground drainage within the Subis Limestone.

4.2. Structural Framework

4.2.1. Lineament Analysis

The lineaments extracted from the SRTM-DEM and ALOS-DSM data (Figure 6) were analysed and rose diagrams were constructed. Two main fracture sets were oriented northeast–southwest, approximately 40–220, and northwest–southwest, approximately 120–300, with local maximum stress (σ_1) in the north–south direction and minimum stress (σ_3) in the east–west direction. The fractures in the northeast and northwest directions are thought to be transtensional, with sinistral shear on the northeast trend and dextral shear on the northwest trend motion. The interpretation of stresses is constrained by the localised data in the study area.

The northeast–southwest trending lineaments follow the hinge line of the anticline and the Trusan Fault, while the northwest–southeast trending lineaments follow the regional fault trends of the Tinjar Line and West Baram Line. The large cavern and passages of the Niah Great Cave Complex are believed to have developed on the northeast–southwest-trending anticline hinge line (Figure 1a) and orientated in the northwest and east–west directions.

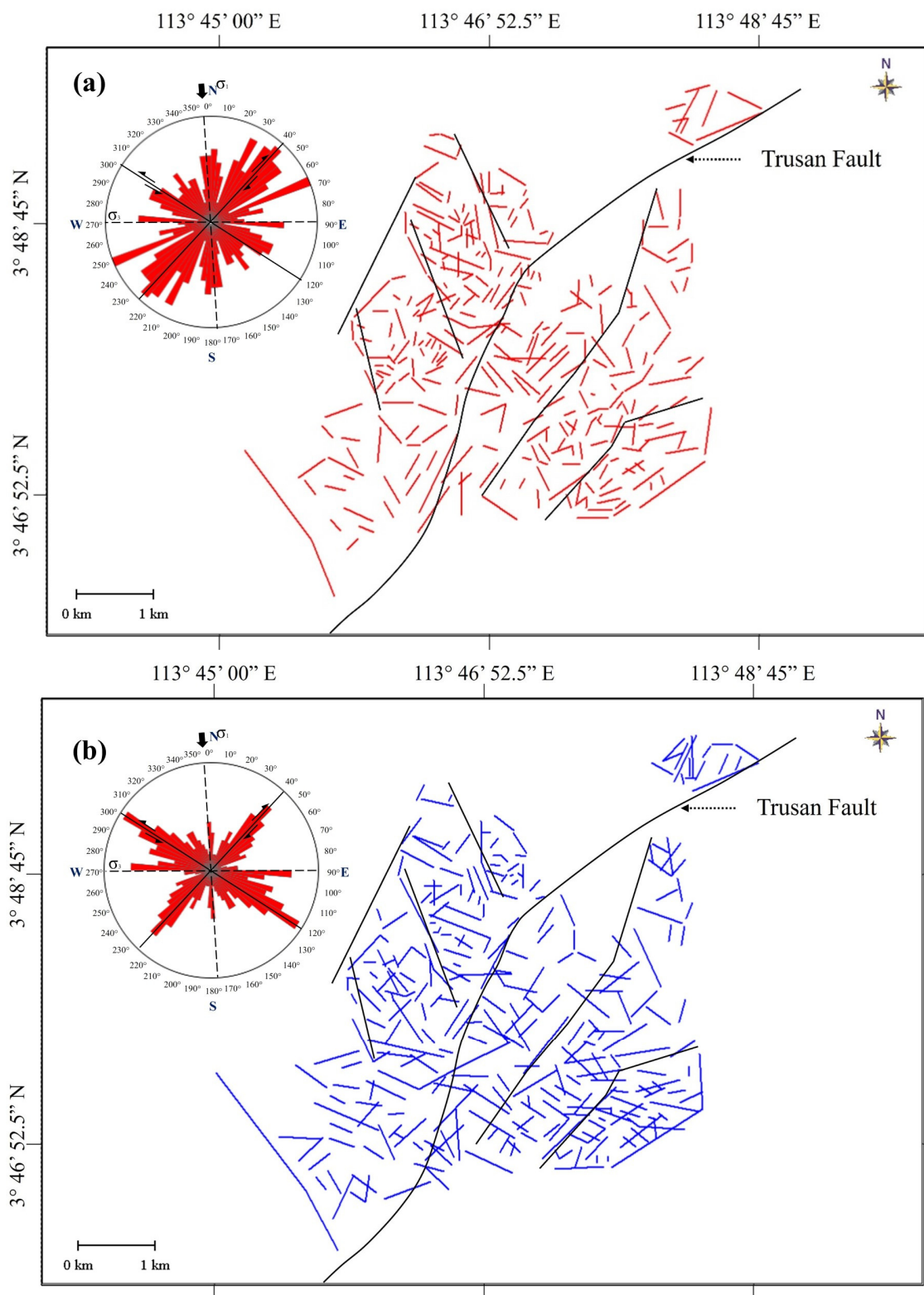


Figure 6. Lineament analysis and rose diagrams from a dataset of (a) SRTM-DEM and (b) ALOS-DSM with a resolution of 30 m. Both lineaments showed similar main fracture sets that were oriented in northeast–southwest and northwest–southeast directions, with north–south-trending compressional stress and extensional stress in the east–west direction. The previously interpreted northeast–southwest dextral Trusan Fault and interpreted faults are shown in black lines [33,65]. The interpretation is strictly based on the localised data in the study area.

4.2.2. Fracture Patterns and Characteristics

Deformation features observed in the outcrops along the timber walkway and caves include conjugate faults/fractures, stylolitic fractures, and extensional mode I fractures (Figure 7). Conjugate faults were observed along the pathway leading from Traders' Cave to the Great Cave (Figure 7a). North–south and northeast–southwest striking fractures with apertures ranging from 30 cm to 1 m were observed on the Painted Cave ceiling and were filled with calcite minerals (Figure 7b). The stalactites formed due to calcite precipitation along the fractures, and there was evidence of dripping water from the ceiling. Additionally, an open west–northwest–east–southeast striking fracture was observed at the southern exit of the Great Cave Complex (Figure 7f). The dissolution process predominantly impacted the limestone's weaker zones, such as the bedding and fractures. Small caves and fractures in the paleo-weathered isolated limestone hill (Figure 7d) indicate an enlargement of the pathway and pore capacity. When dissolution along the vertical fractures reached its limit, the cave ceiling collapsed, forming the dolines or sinkholes with boulder fragments on the cave floor (Figure 7e).

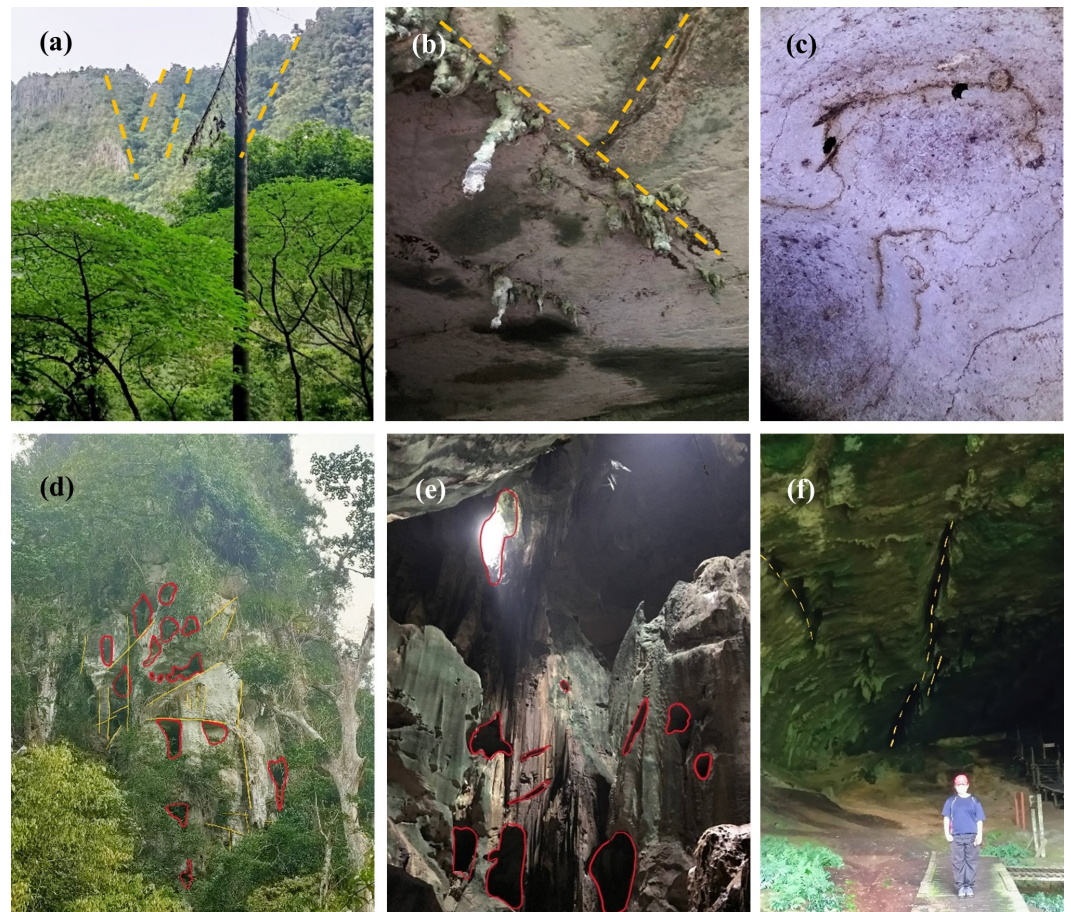


Figure 7. (a) Conjugate faults observed along the walkway from Traders' Cave to the Great Cave. (b) Calcite-filled fractures on the ceiling of Painted Cave with strike trending in north–south and northeast–southwest directions. Stalactite formation was observed due to precipitation via the fractures. (c) Stylolite fractures in the Great Cave. (d) Enhanced fractures due to dissolution on the isolated limestone hill. (e) Doline and the dissolved cavities with the majority of vertical fractures. (f) Large west–northwest–east–southeast striking vertical fractures at the exit of the Great Cave in the south.

4.3. Karst Features Delineation

4.3.1. Karst Depression

This study identified 79 potential dolines or karst depressions by visualising the SRTM-DEM in the Niah–Subis build-up (Figure 8a). The largest doline (0.147 km²) was found in the middle of the paleo-karst build-up, while the smallest doline (9.8 m²) was found closer to the surface river network (Figure 8b). The doline size distribution demonstrates the inter-relationship between the surface and underground drainage systems in the development of karstic processes. The subsurface drainage dissolved the subaerial limestone build-up, causing the ceiling of the structure to collapse. On the topography map, it appears as a closed depression (Figure 8a). The Niah regional lineaments and doline distribution were compared (Figure 8b), demonstrating that the larger dolines were bounded or intersected by lineaments of greater intensity.

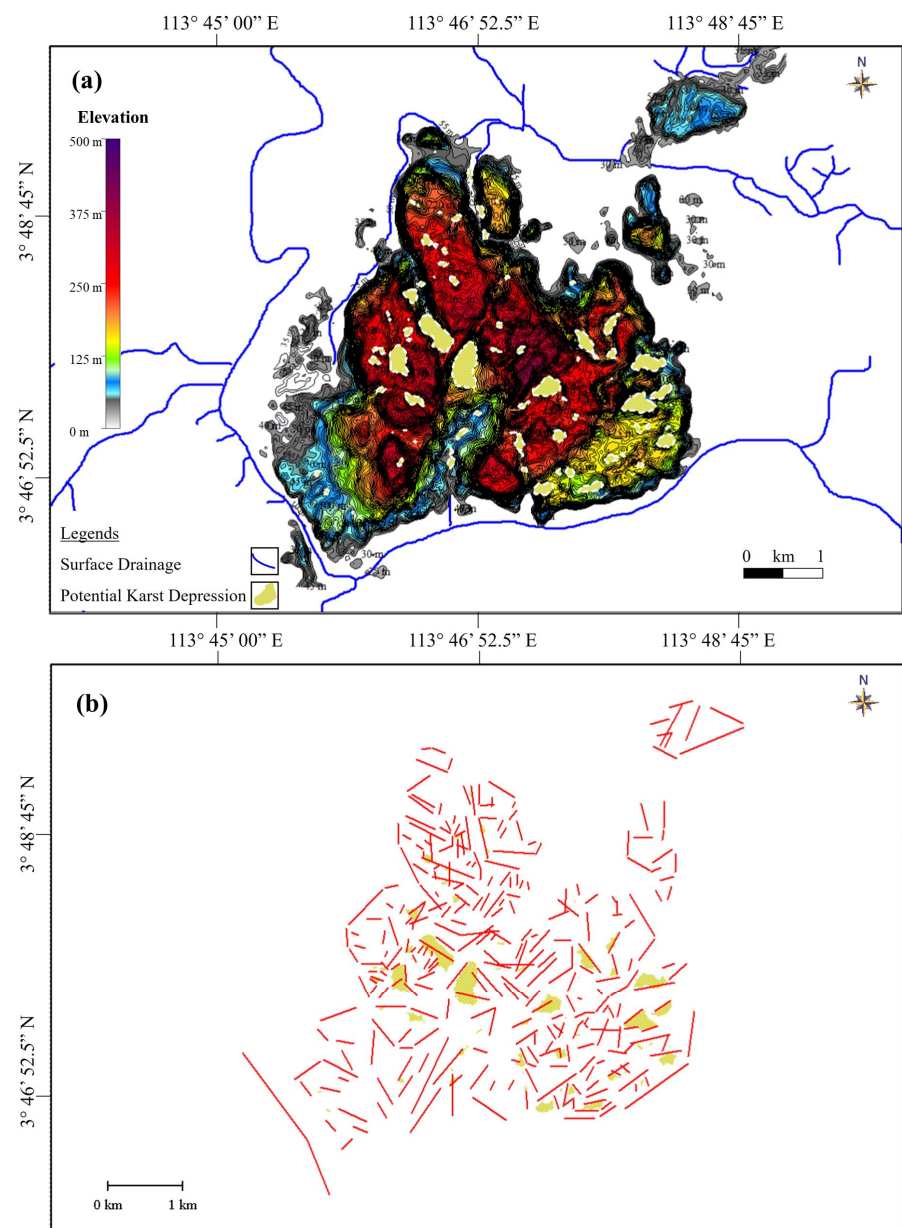


Figure 8. (a) Potential karst depression identified from the DEM (yellow shapes) and topography map with surrounding surface drainage system (blue lines). (b) Regional lineaments (red lines) and the potential karst depression (yellow shapes).

4.3.2. Karst Features in Outcrops

Based on the geological observations made during the fieldwork, the karst features observed in the field are categorised into several characteristics and features. These characteristics are as follows:

1. Isolated limestone hill: Formed due to paleo-weathering and dissolution (Figure 9a).
2. Cavern with stalagmites, stalactites, and pillars: Formed due to calcite precipitation (Figure 9c,e,f).
3. Vertical grooves: Formed due to dissolution (Figure 9d).
4. Water table: Formed due to the dissolution and erosion by the drainage leaving the hard bedrock (Figure 9g).

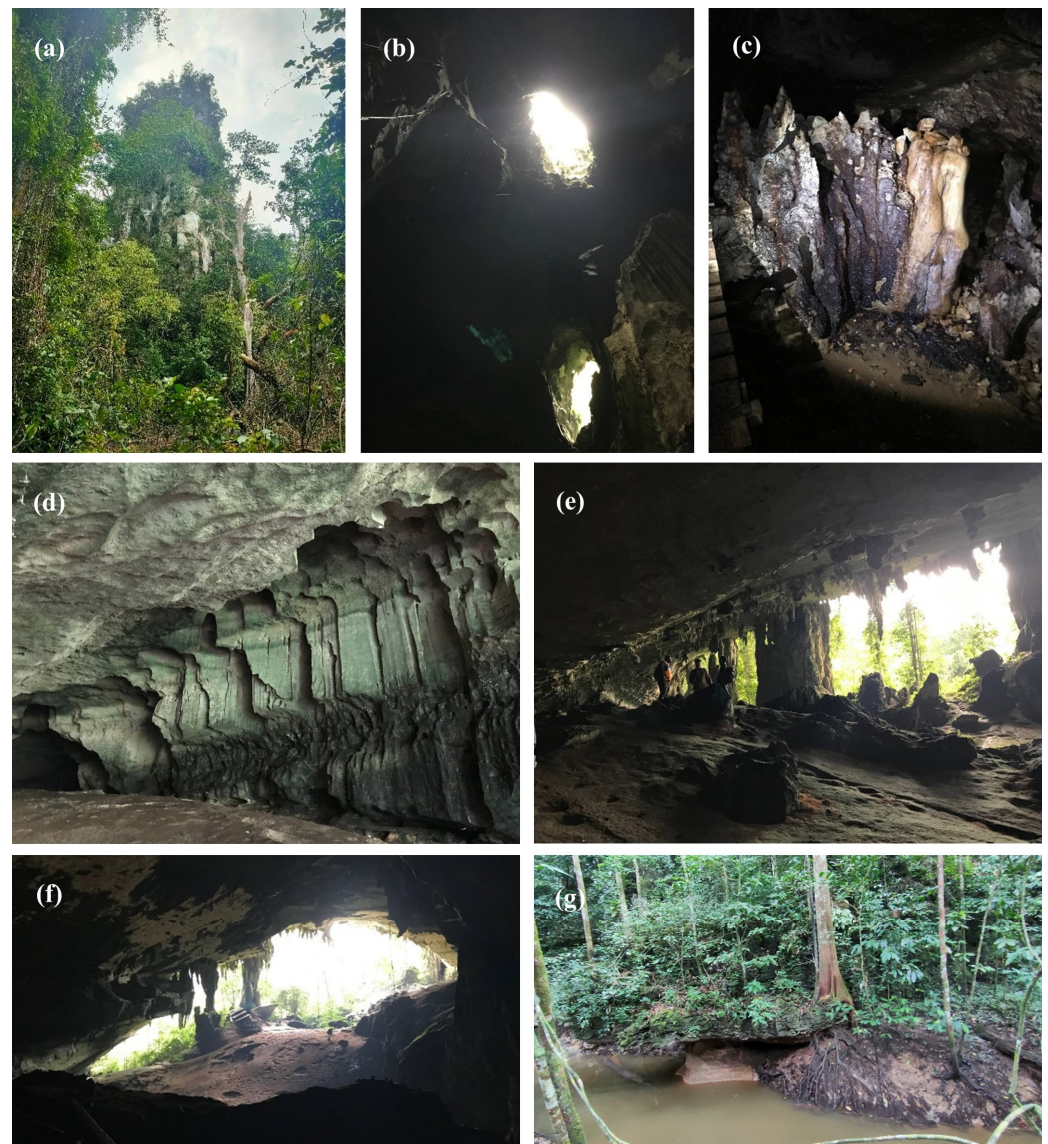


Figure 9. (a) Isolated limestone hill. (b) Dolines in the ceiling of Great Cave. (c) Active stalagmites. (d) Vertically dissolution-enhanced groove of Great Cave. (e) Inclined ceiling of the Traders' Cave with boulders. (f) General view of one of the entrances of the Great Cave with pillars. (g) Stream along the timber walkway towards the cave entrance with the appearance of a water table.

4.4. Karst Network Modelling and Topology Analysis

4.4.1. Discrete Fracture Network Modelling (DFN)

Due to limited accessibility to the outcrops, the 2D DFNs were only constructed following the regional lineaments of the Subis build-up and open fractures at the southern exit of the Great Cave. Nodes in black circles and trace mid-points in red circles were used to represent the traces (Figures 10b and 11b).

4.4.2. Fracture Network Topology

Fracture Length Distribution

Figures 10c and 11c showed the trace length distribution in two different scale datasets. Both histograms illustrate a wide range of lengths and a comparable unimodal distribution of fracture trace lengths with a positive skew. The most abundant lineament lengths vary from 150 m to 225 m, whereas the dominant outcrop-scale fracture lengths range from 0.7 cm to 1.4 cm.

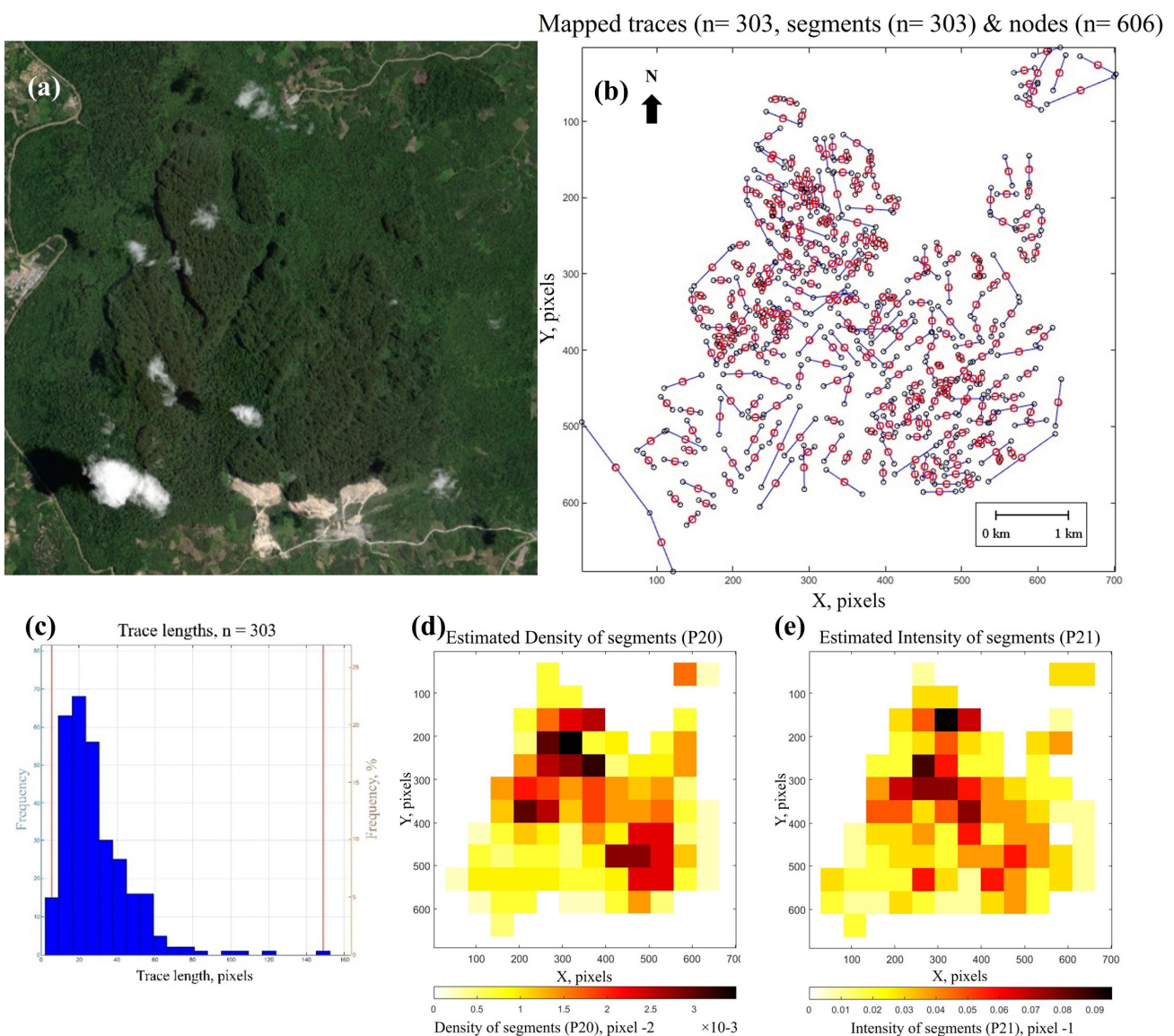


Figure 10. (a) Satellite image of Subis build-up covered by high-intensity of vegetation. (b) Two-dimensional DFN model based on the lineament traces. Nodes in black circles and trace mid-points in red circles were used to represent the traces. (c) Length distribution. (d) Estimated density of the fractures (P20). (e) Estimated intensity of fractures (P21) [scale: 100 pixels = 1 km].

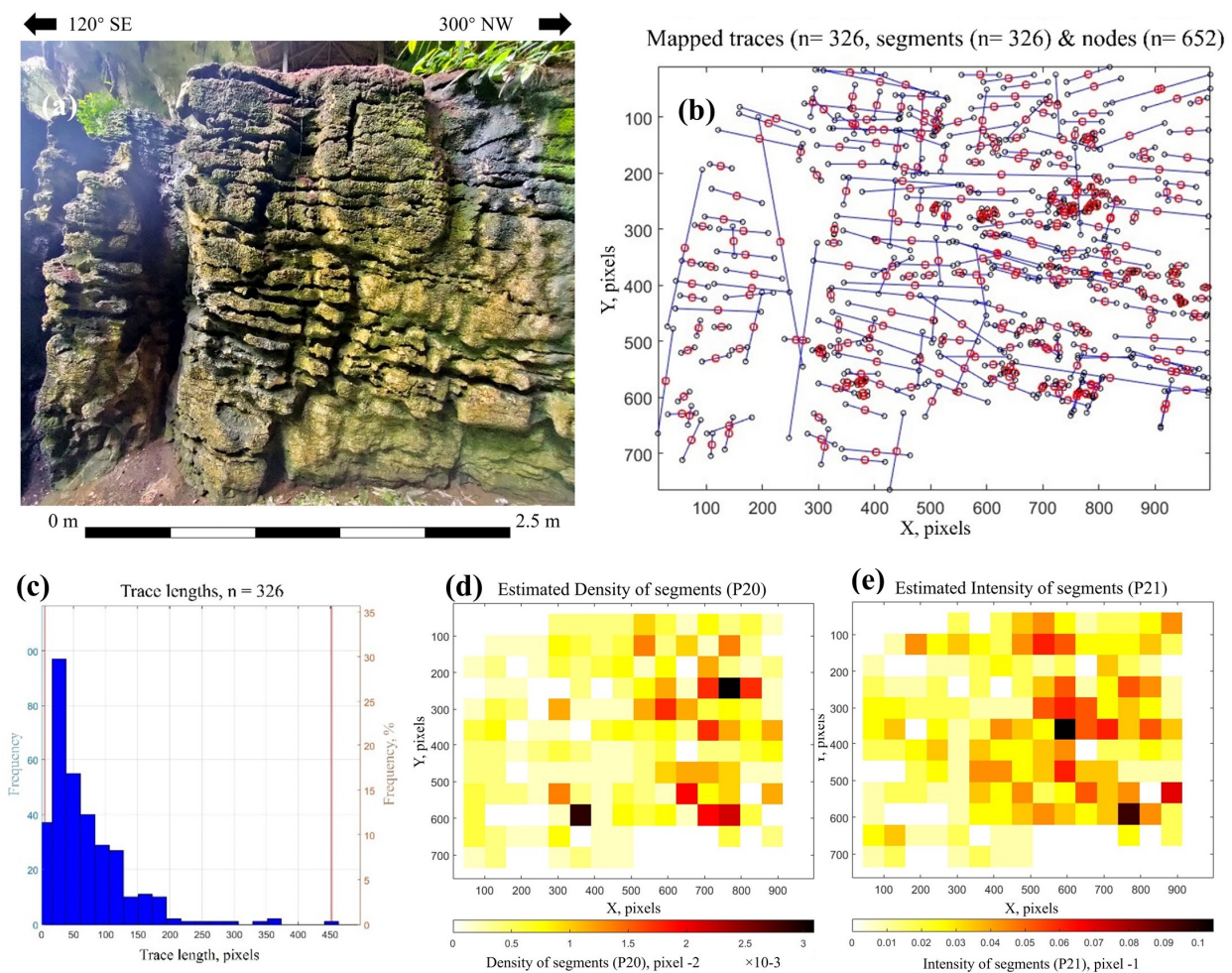


Figure 11. (a) Enlarged open fractures due to dissolution. (b) Two-dimensional DFN model based on the outcrop-scale fracture traces. Nodes in black circles and trace mid-points in red circles were used to represent the traces. (c) Length distribution. (d) Estimated density of the fractures (P20). (e) Estimated intensity of fractures (P21) [scale: 800 pixels = 2.5 m].

Fracture Density (P20), Intensity (P21), and Connectivity (I–X–Y)

Figure 10d,e and Figure 11d,e depict the fracture density (P20), which represents the number of fractures per unit area, as well as the intensity (P21), which reflects the total length of fractures per unit area. For examination purposes, both regional- and outcrop-scale traces were confined by a square box. The northern part of the Subis Limestone build-up had the most fractures and the longest overall length of fractures. Meanwhile, the outcrop-scale fractures were denser in the northwest direction of the outcrop. These two parameters, however, cannot be used directly in the 3D fracture modelling as they are directionally dependent on either the measurements or on boundary sensitivity.

The I–X–Y topology was analysed to quantify the connectivity of the fracture networks and is represented by the average number of connections per line (C_L). Sanderson and Nixon [56] described the values of two contour lines. Lineaments at the regional scale (Figure 12a–d) and fractures at the outcrop scale (Figure 12e,h) were interpreted. The triangular plots depict the detailed topological analyses of nodes and branches for regional- and outcrop-scale fractures, as indicated by the fracture network's relative proportions of isolated (I), splay or abutment (Y), and intersection (X) nodes.

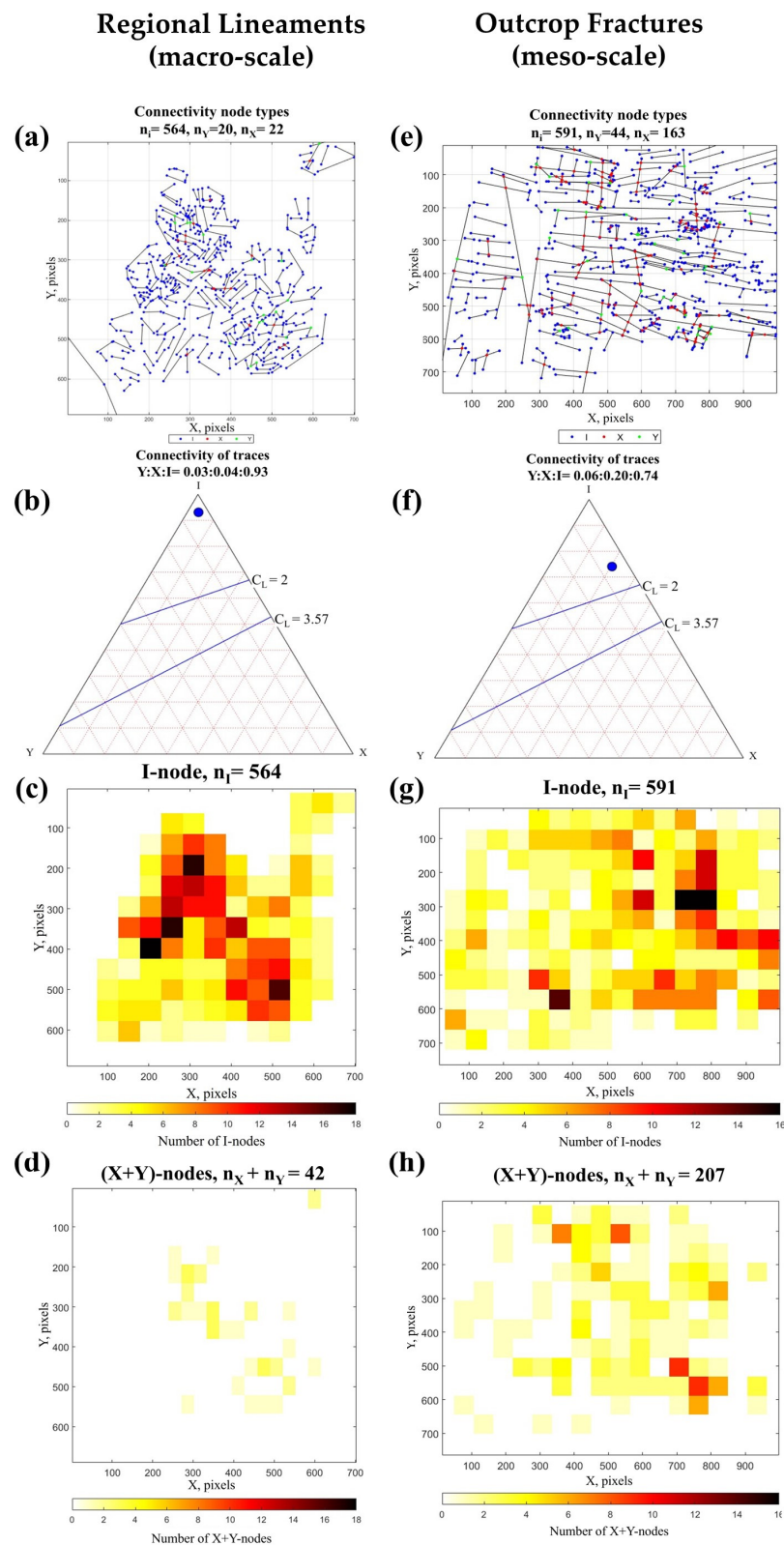


Figure 12. The connectivity of traces (isolated (I), splay or abutment (Y), and intersection (X) for regional lineaments (a–d) and outcrop fractures (e,h). A ternary plot of fracture segment connectivity (b,f) lineaments and fracture traces on (a,e). (c,g) Heat maps of I nodes and (d,h) X + Y nodes.

Based on the I–X–Y models for the dataset utilised in this study, I nodes or isolated nodes are the predominant node type for the regional scale lineaments ($I = 0.93$) with

relatively low values in the X–Y or intersection-abutment nodes ($X = 0.04$, $Y = 0.03$). Similarly, at the outcrop scale, the dominant type of nodes are I nodes ($I = 0.74$) with comparatively low values in the X–Y nodes ($X = 0.20$, $Y = 0.06$). The heat maps of X + Y nodes for both scales in the Subis Limestone reveal a low proportion of X + Y nodes, indicating that the fracture patterns are poorly connected (Figure 12d,h). According to the results of the I–X–Y connectivity models, naturally fractured reservoirs are characterised by isolated fractures with poor connectivity, without considering the karst-related porosity effect on the fracture.

5. Results

5.1. Fracture Network Characteristics

A more comprehensive interpretation of the Subis build-up fracture network was performed based on the structural geology investigation of the outcrop and lineament analysis. The fracture length distribution and fracture network connection appear to be independent of scale and location. Regional lineaments and local fractures reflect an I-node's dominance, implying that the fractures are isolated and rarely connected.

When the fracture length and connectivity are compared, the fracture set orientation shows scale-dependent and spatial differences. The west–northwest–east–southeast trending open fractures in the southern exit of the Great Cave followed the extension direction. In contrast, the fractures in the Painted Cave followed the main fault direction (Trusan Fault). The fracture density and the intensity are prone to significant lateral changes, which might be influenced by regional tectonic structures, especially the uplift and compressional events that occurred from the Late Miocene to Early Pliocene periods [47].

The scale and resolution of the data are crucial factors in generating the results. Because data resolution varies, the estimation of fracture network parameters, such as fracture connectivity, is affected by both the scale aspect and the resolution limits of the data source for DFN modelling. The fracture connectivity between the outcrop and the regional analysis demonstrated that the fractures detected are isolated, with minimal intersection seen via the X-nodes (intersection nodes). However, the number of intersection nodes increases when the resolution is increased to a centimetre–metre scale. Limited access to outcrops within the whole Niah–Subis Limestone complex is indeed one of the influential factors for the outcome presented in this paper. Given the difficult accessibility of exposed Miocene limestone outcrops in onshore north Sarawak, the Niah–Subis Limestone complex/build-up is sufficient to meet the goal of this study, namely, to perform a multi-scale analysis (macro- and meso-scale) to understand the complexity of naturally fractured networks in karstified carbonates.

5.2. Relationship between the Fracture Network and Karstification

Due to the influence of significant compressive stress, an anticline structure is a favourable zone for karst development in the axial section of the structure. A series of faults and fractures evolved in the direction parallel to the anticline hinge during the formation of the anticline. Since fractures are prone to karstification, the karst features developed along the weak fracture paths, particularly where the fracture sets intersected.

In the Subis Limestone build-up, potential karst depressions are distributed around the fracture zones (Figure 8), indicating that their formations are strongly associated with the faults and fractures. Surface and underground water infiltrates along faults and fractures, dissolving the carbonate along the pathway. Dissolution pores along the fractures formed in the early stages can enhance the porosity and permeability of the carbonate reservoirs. Large-scale caves easily form at the intersection of multiple groups of faults or fractures. For instance, the orientation of the passages of the Great Cave and the north–south trending isolated passage of the Traders' Cave match the major regional lineament sets.

The studied outcrop has well-developed fractures, vugs, caves, and passages, which can become potential pathways or capacities for the reservoirs if they are unfilled, semi-filled, or filled with permeable sediments. The connectivity of the fracture network

can be enhanced or reduced by considering the interplay of the matrix porosity in the DFN modelling.

The observed fractures were mainly infilled by calcite minerals, with some passages and caves being partially filled by boulders. Large limestone boulders were found in the southern part of the Traders' Cave and were thought to represent the remains of the collapsed ceiling during the karst maturation phase. The cave is open to the east, which is believed to be caused by paleo-weathering at the north–south trending cliff. The boulders at the bottom of the dolines provided similar evidence of ceiling collapse (dolines) in the Great Cave. The collapse event in karst structures is a process of karst maturation that continues until the erosional process is complete. Karst dissolution primarily occurs along the fractures and enlarges the pathway through time.

In offshore carbonate build-ups, the void system and karst caverns partially collapse during subsequent burial, potentially resulting in karst-related traps. Using the Subis Limestone near-surface karst system as an analogue, the karst cavern zones in Central Luconia are likely to extend horizontally rather than vertically while oriented parallel to major structural lineaments.

5.3. Implication for Geological Carbon Storage and Naturally Fractured Reservoirs

Central Luconia carbonate reservoirs are promising sites for carbon storage as they meet the critical criteria, such as being located within the seismic-free zone, possessing suitable geothermal conditions [2,3], and experiencing minimal active faulting. Although active faulting is minimal, paleo-faults are prevalent within the Cenozoic sections, particularly in the Oligocene–Miocene sequences. Thus, analysing the fracture network characteristics in assessing the reservoir's carbon storage capability is crucial. Carbon storage in carbonate reservoirs must be evaluated while considering the presence of secondary karst-related porosity. Modelling a realistic fracture network that integrates secondary karst-related porosity, on the other hand, is difficult, especially when there is a lack of available borehole data and the carbon storage volume in the reservoirs needs to be estimated. By studying the outcrop analogues, the behaviour of small (centimetre) and intermediate (metre) scale fracture networks can be acquired by combining outcrop and DEMs. Simultaneously, their interaction with karst features can be physically observed in the field. Areas that appear to lack faults or fractures on the seismic scale may be fractured on smaller scales. The smaller-scale fracture network is predicted to have better connectivity than the seismic-scale fractures. Underestimation of the fracture network can occur if the sub-seismic scale fractures are overlooked.

The apertures of the fractures primarily determine the permeability of the reservoirs. Fracture orientation and density also affect the permeability, albeit to a lesser extent. According to the 2D DFN models constructed in the Subis Limestone paleo-karst system, only a minor part of the total fracture network contributes to the connectivity. According to field observations, the degree of the fracture enlargement or aperture and secondary porosity (e.g., vugs, caves) is vital for predicting the behaviour of karstified fracture reservoirs, as the significant secondary porosity in the carbonates could be an option for the long-term storage of carbon dioxide [40]. The degree of fracture enlargement in offshore carbonates can be extracted from the borehole log images, well test analysis, and/or mud loss drilling information.

The analysis provided in this analogue study can be further applied to support the quantitative characterisation of fractures in naturally fractured carbonate reservoirs at multiple scales to improve the qualitative interpretation of the fracture network.

6. Conclusions

Overall, the fracture analysis conducted on the Niah–Subis Limestone complex provides an excellent analogue study for the Oligocene–Miocene carbonate reservoirs in Central Luconia Province. Using DEM data and outcrop observations, the combination of lineament analysis and karst features was analysed and delineated. The properties of

fractures were then compared at both the regional (macro-scale) and outcrop (meso-scale) levels using 2D DFN models and topology analysis. The findings of this paper have concluded that:

- a. Integrating the outcrop and regional lineament analysis allows for a more detailed description and characterisation of the sub-seismic scale complex fracture network and can reduce the observational gap between well and seismic data;
- b. Karst features such as dolines, caves, passages, and speleothems are highly influenced by the intersection of fractures, major orientations, and the surface and underground drainage systems. The paleo-karst fracture networks are also strongly impacted by karst dissolution;
- c. Fracture parameters, including length distribution, density, intensity, and connectivity, are mainly scale-independent and vary spatially;
- d. Both regional lineament and outcrop fracture analyses in this study demonstrate that the fractures are isolated, with little connectivity between them. This should be reconsidered as limitations on outcrop accessibility can influence the results of the I-X-Y model;
- e. The small contribution of total fractures to the fracture network connectivity and the discrete behaviour of paleo-karst fractures has emphasised the importance of incorporating the matrix porosity across multiple scales of fracture network modelling in future studies. This should be performed for a better solution in upscaling the fracture–vug network model and to reduce the underestimation of models;
- f. Lastly, the fracture network models can predict the fluid flow and the potential karst feature alignment by incorporating the reservoirs' permeability and porosity.

Author Contributions: Conceptualization, P.Y.O. and S.N.F.J.; methodology, P.Y.O.; software, P.Y.O.; validation, P.Y.O. and S.N.F.J.; formal analysis, P.Y.O.; investigation, P.Y.O. and S.N.F.J.; resources, S.N.F.J.; data curation, P.Y.O. and S.N.F.J.; writing—original draft preparation, P.Y.O.; writing—review and editing, S.N.F.J.; visualization, P.Y.O.; supervision, S.N.F.J.; project administration, P.Y.O. and S.N.F.J.; funding acquisition, S.N.F.J. All authors have read and agreed to the published version of the manuscript.

Funding: This research was funded by the YUTP-FRG Grant entitled Assessment of CO₂ Storage Potential in Naturally Fractured Carbonate Reservoir Through DFN and Dual-Porosity (Seismic) Model with the Cost Centre 015LC0-466 under Yayasan Universiti Teknologi PETRONAS (YUTP).

Institutional Review Board Statement: Not applicable.

Informed Consent Statement: Not applicable.

Data Availability Statement: Restrictions apply to the availability of the data.

Acknowledgments: The work contained in this paper is part of a PhD research project supported by the Centre for Subsurface Imaging (CSI), Universiti Teknologi PETRONAS, which provided research facilities and supported during fieldwork in Niah, Sarawak on February, 2023, with a research fund under cost centres of 015LC0-466 (YUTP-FRG) and 015PBC-021 (YUTP-PRG). The authors [62] also acknowledge the open-source tool FracPaQ version 2.8 for its use in fracture topology analysis.

Conflicts of Interest: The authors declare no conflict of interest.

References

1. Jamaludin, S.N.F.; Sautter, B.; Pubellier, M.; Beg, M.A. The Succession of Upper Eocene-Upper Miocene Limestone Growth and Corresponding Tectonic Events in Luconia Shelf, Sarawak, Malaysia. *Front. Earth Sci.* **2021**, *9*, 588629. [[CrossRef](#)]
2. Hasbollah, D.Z.A.; Junin, R. Assessment of geological CO₂ storage potential in central Luconia province. *Int. J. Adv. Appl. Sci.* **2017**, *4*, 44–48. [[CrossRef](#)]
3. Junin, R.; Hasbollah, D. A Preliminary Basin Scale Evaluation Framework of Potential Sedimentary Basins in Malaysia for Carbon Dioxide Sequestration. In Proceedings of the Conference on Process Integration, Modelling and Optimisation for Energy Saving and Pollution Reduction (PRES), Kuching, Malaysia, 23–27 August 2015; pp. 1537–1542.
4. Gholami, R.; Raza, A.; Iglauer, S. Leakage risk assessment of a CO₂ storage site: A review. *Earth-Sci. Rev.* **2021**, *223*, 103849. [[CrossRef](#)]

5. Rasool, M.H.; Ahmad, M.; Ayoub, M. Selecting Geological Formations for CO₂ Storage: A Comparative Rating System. *Sustainability* **2023**, *15*, 6599. [[CrossRef](#)]
6. Ajayi, T.; Gomes, J.; Bera, A. A review of CO₂ storage in geological formations emphasizing modeling, monitoring and capacity estimation approaches. *Pet. Sci.* **2019**, *16*, 1028–1063. [[CrossRef](#)]
7. Raza, A.; Rezaee, R.; Gholami, R.; Rasouli, V.; Bing, C.H.; Nagarajan, R.; Hamid, M.A. Injectivity and quantification of capillary trapping for CO₂ storage: A review of influencing parameters. *J. Nat. Gas Sci. Eng.* **2015**, *26*, 510–517. [[CrossRef](#)]
8. Yu, J.; Li, Z.; Yang, L. Fault system impact on paleokarst distribution in the Ordovician Yingshan Formation in the central Tarim basin, northwest China. *Mar. Pet. Geol.* **2016**, *71*, 105–118. [[CrossRef](#)]
9. Lopes, J.A.; Medeiros, W.E.; La Bruna, V.; de Lima, A.; Bezerra, F.H.; Schiozer, D.J. Advancements towards DFKN modelling: Incorporating fracture enlargement resulting from karstic dissolution in discrete fracture networks. *J. Pet. Sci. Eng.* **2022**, *209*, 109944. [[CrossRef](#)]
10. Uematsu, H.; Auxiette, G.; Bellah, S.; Virlan, V.; Stojic, T. New approach using dual porosity dual permeability and dissolved pore network to simulation modeling for fractured carbonate reservoir in Abu Dhabi. In Proceedings of the Abu Dhabi International Petroleum Exhibition & Conference, Abu Dhabi, United Arab Emirates, 13–16 November 2017.
11. Akram, A.H.; Gherryo, Y.S.; Ali, S.; Thabt, M.S.; Serban, A. Dynamic behavior of a fissured dual-carbonate reservoir modeled with DFN. In Proceedings of the North Africa Technical Conference and Exhibition, Cairo, Egypt, 14–17 February 2010.
12. Loucks, R.G. Paleocave carbonate reservoirs: Origins, burial-depth modifications, spatial complexity, and reservoir implications. *AAPG Bull.* **1999**, *83*, 1795–1834. [[CrossRef](#)]
13. Volatili, T.; Agosta, F.; Cardozo, N.; Zambrano, M.; Lecomte, I.; Tondi, E. Outcrop-scale fracture analysis and seismic modelling of a basin-bounding normal fault in platform carbonates, central Italy. *J. Struct. Geol.* **2022**, *155*, 104515. [[CrossRef](#)]
14. Espejel, R.L.; Alves, T.M.; Blenkinsop, T.G. Multi-scale fracture network characterisation on carbonate platforms. *J. Struct. Geol.* **2020**, *140*, 104160. [[CrossRef](#)]
15. Gutmanis, J.; I Oró, L.A.; DiEz-Canseco, D.; Chebbihi, L.; Awdal, A.; Cook, A. Fracture analysis of outcrop analogues to support modelling of the subseismic domain in carbonate reservoirs, south-central Pyrenees. In *Geological Society, London, Special Publications*; The Geological Society: London, UK, 2018; Volume 459, pp. 139–156.
16. Agosta, F. Some open issues in the analysis of the storage and migration properties of fractured carbonate reservoirs. In Proceedings of the EGU General Assembly Conference, Vienna, Austria, 23–28 April 2017; p. 6741.
17. Lohr, T. Seismic and Sub-Seismic Deformation on Different Scales in the NW German Basin. Ph.D. Thesis, Deutsches Geo-ForschungsZentrum GFZ, Potsdam, Germany, 2007; pp. 35–48. [[CrossRef](#)]
18. Narr, W.; Schechter, D.S.; Thompson, L.B. *Naturally Fractured Reservoir Characterization*; Society of Petroleum Engineers: Richardson, TX, USA, 2006; Volume 112.
19. Lonergan, L.; Jolly, R.; Rawnsley, K.; Sanderson, D. *Fractured Reservoirs*; Geological Society: London, UK, 2007. [[CrossRef](#)]
20. Odling, N.E. Scaling and connectivity of joint systems in sandstones from western Norway. *J. Struct. Geol.* **1997**, *19*, 1257–1271. [[CrossRef](#)]
21. Maerten, L.; Gillespie, P.; Daniel, J.-M. Three-dimensional geomechanical modeling for constraint of subseismic fault simulation. *AAPG Bull.* **2006**, *90*, 1337–1358. [[CrossRef](#)]
22. Giuffrida, A.; La Bruna, V.; Castelluccio, P.; Panza, E.; Rustichelli, A.; Tondi, E.; Giorgioni, M.; Agosta, F. Fracture simulation parameters of fractured reservoirs: Analogy with outcropping carbonates of the Inner Apulian Platform, southern Italy. *J. Struct. Geol.* **2019**, *123*, 18–41. [[CrossRef](#)]
23. Kokkalas, S.; Vakalas, I.; Jones, R. Fracture density variation at different observation scales in carbonate reservoir outcrop analogues. In Proceedings of the EAGE Middle East Geomechanics Workshop: Lessons Learned & New Frontiers, Online, 1–3 March 2022; Volume 2022, pp. 1–5. [[CrossRef](#)]
24. Dodge-Wan, D.; Viswanathan, P.M.; Ramasamy, N.; Arumugam, A. Epiphreatic caves in Niah karst tower (NW Borneo): Occurrence, morphology and hydrogeochemistry. *Acta Carsologica* **2017**, *46*, 149–163. [[CrossRef](#)]
25. Ramkumar, M.; Nagarajan, R.; Mathew, M.J.; Sautter, B.; Siddiqui, N.A.; Saw, B.B.; Santosh, M.; Menier, D.; Poppelreiter, M.C. Relict hydrocarbon seeps in the Oligocene-Miocene Subis carbonate platform, Malaysia: Implications on hydrocarbon generation and migration pathways and potential sealing by shale gouging. *Geol. J.* **2021**, *56*, 2571–2582. [[CrossRef](#)]
26. Fournillon, A.; Fournier, F.; Vidal, O. Seismic expression of carbonate build-up karstification: Karst modelling strategies and insights from synthetic seismic. *Geol. Soc. Lond. Spec. Publ.* **2021**, *509*, 227–248. [[CrossRef](#)]
27. Saw, B.B.; Schlaich, M.; Poppelreiter, M.C.; Ramkumar, M.; Lunt, P.; Vintaned, J.A.G.; Ali, S.H. Facies, depositional environments, and anatomy of the Subis build-up in Sarawak, Malaysia: Implications on other Miocene isolated carbonate build-ups. *Facies* **2019**, *65*, 28. [[CrossRef](#)]
28. Rankey, E.C.; Schlaich, M.; Mokhtar, S.; Ghon, G.; Ali, S.H.; Poppelreiter, M. Seismic architecture of a Miocene isolated carbonate platform and associated off-platform strata (Central Luconia Province, offshore Malaysia). *Mar. Pet. Geol.* **2019**, *102*, 477–495. [[CrossRef](#)]
29. Dedeche, A.S.; Pierson, B.J.; Hunter, A.W. Growth History and Facies Evolution of the Subis Limestone—A Carbonate Platform Exposed Onshore Borneo Island, Malaysia. In Proceedings of the 75th EAGE Conference & Exhibition Incorporating SPE EUROPEC 2013, London, UK, 10–13 June 2013. [[CrossRef](#)]

30. Dodge-Wan, D.; Deng, A.H.M.; Abbas, M.F. Occurrence and morphology of crayback-like stalagmites in the Painted Cave of Niah (Sarawak, Malaysia). *Carbonates Evaporites* **2012**, *27*, 343–356. [CrossRef]
31. McFarlane, D.A. A Note on the Occurrence of a Crayback Stalagmite at Niah Caves, Borneo. *Int. J. Speleol.* **2011**, *40*, 39–43. [CrossRef]
32. Dodge-Wan, D. The Traders' Cave of Niah (NW Borneo): Morphology and features as indicators of speleogenesis and karstification. *Carbonates Evaporites* **2018**, *33*, 315–329. [CrossRef]
33. Hutchison, C.S. *Geology of North-West Borneo: Sarawak, Brunei and Sabah*; Elsevier: Amsterdam, The Netherlands, 2005.
34. Tongkul, F. Regional geological correlation of Paleogene sedimentary rocks between Sabah and Sarawak. *Bull. Geol. Soc. Malays.* **1999**, *43*, 31–39. [CrossRef]
35. Ali, M.Y. An integrated analysis of the depositional control, sedimentology and diagenesis of Cenozoic carbonates from the Sarawak basin, east Malaysia. Ph.D. Thesis, Imperial College London, London, UK, 2014.
36. Madon, M.; Kim, C.L.; Wong, R. The structure and stratigraphy of deepwater Sarawak, Malaysia: Implications for tectonic evolution. *J. Asian Earth Sci.* **2013**, *76*, 312–333. [CrossRef]
37. Hall, R. Cenozoic plate tectonic reconstructions of SE Asia. *Geol. Soc. Lond. Spec. Publ.* **1997**, *126*, 11–23. [CrossRef]
38. Hall, R. Cenozoic geological and plate tectonic evolution of SE Asia and the SW Pacific: Computer-based reconstructions, model and animations. *J. Asian Earth Sci.* **2002**, *20*, 353–431. [CrossRef]
39. Hutchison, C.S. Marginal basin evolution: The southern South China Sea. *Mar. Pet. Geol.* **2004**, *21*, 1129–1148. [CrossRef]
40. Ali, S.H.; Poppelreiter, M.C.; Saw, B.B.; Shah, M.M.; Bashir, Y. Facies, diagenesis and secondary porosity of a Miocene reefal platform of Central Luconia, Malaysia. *Carbonates and Evaporites* **2021**, *36*, 1–25. [CrossRef]
41. Yusliandi, A.; Sautter, B.; Poppelreiter, M.C. The various controls on the platform architecture of carbonate buildups in the Central Luconia Province, Offshore Sarawak. *Pet. Coal* **2019**, *61*, 1425–1437.
42. Metcalfe, I. Tectonic framework and Phanerozoic evolution of Sundaland. *Gondwana Res.* **2011**, *19*, 3–21. [CrossRef]
43. Koša, E.; Warrlich, G.M.; Loftus, G. Wings, mushrooms, and Christmas trees: The carbonate seismic geomorphology of Central Luconia, Miocene–present, offshore Sarawak, northwest Borneo. *AAPG Bull.* **2015**, *99*, 2043–2075. [CrossRef]
44. Sahari, S.; Ahmad Shah, A.; Aaisyah, D.; Batmanathan, N.; Shahbuddin, A. Active detachment faulting controls folding and faulting in western Borneo, SE Asia. *J. Asian Earth Sci.* **2023**, *9*, 100133. [CrossRef]
45. Lin, Y.A.; Colli, L.; Wu, J.; Schuberth, B.S. Where are the proto-South China Sea slabs? SE Asian plate tectonics and mantle flow history from global mantle convection modeling. *J. Geophys. Res. Solid Earth* **2020**, *125*, e2020JB019758. [CrossRef]
46. Wang, P.C.; Li, S.Z.; Guo, L.L.; Jiang, S.H.; Somerville, I.D.; Zhao, S.J.; Zhu, B.D.; Chen, J.; Dai, L.M.; Suo, Y.H.; et al. Mesozoic and Cenozoic accretionary orogenic processes in Borneo and their mechanisms. *Geol. J.* **2016**, *51*, 464–489. [CrossRef]
47. Kessler, F.L.; Jong, J. Paleogeography and carbonate facies evolution in NW Sarawak from the Late Eocene to the Middle Miocene. *War. Geol.* **2016**, *42*, 1–9.
48. Moss, S. Embaluh Group turbidites in Kalimantan: Evolution of a remnant oceanic basin in Borneo during the Late Cretaceous to Palaeogene. *J. Geol. Soc.* **1998**, *155*, 509–524. [CrossRef]
49. Cullen, A.B. Transverse segmentation of the Baram-Balabac Basin, NW Borneo: Refining the model of Borneo's tectonic evolution. *Pet. Geosci.* **2010**, *16*, 3–29. [CrossRef]
50. Cullen, A. Nature and significance of the West Baram and Tinjar Lines, NW Borneo. *Mar. Pet. Geol.* **2014**, *51*, 197–209. [CrossRef]
51. Zheng, Q.L.; Li, S.Z.; Suo, Y.H.; Li, X.Y.; Guo, L.L.; Wang, P.C.; Zhang, Y.; Zang, Y.B.; Jiang, S.H.; Somerville, I.D. Structures around the Tinjar-West Baram Line in northern Kalimantan and seafloor spreading in the proto-South China Sea. *Geol. J.* **2016**, *51*, 513–523. [CrossRef]
52. Sleumer, B. The Subis Limestone Complex—Sarawak, Malaysia. In Proceedings of the Carbonate Seminar, Special, Indonesia Petroleum Association, Jakarta, Indonesia, 12–19 September 1976. Volume 120.
53. Agostinelli, E.; bin Ahmad Tajuddin, M.R.; Antonielli, E.; bin Mohd Aris, M. Miocene-Pliocene paleogeographic evolution of a tract of Sarawak offshore between Bintulu and Miri. *Geol. Soc. Malays. Bull.* **1990**, *27*, 117–135. [CrossRef]
54. Welch, M.J.; Lüthje, M.; Oldfield, S.J. *Modelling the Evolution of Natural Fracture Networks*; Springer: Berlin/Heidelberg, Germany, 2020; Volume 965.
55. Mendes, L.d.C.; Correia, U.M.; Cunha, O.R.; Oliveira, F.M.; Vidal, A.C. Topological analysis of fault network in naturally fractured reservoirs: A case study from the pre-salt section of the Santos Basin, Brazil. *J. Struct. Geol.* **2022**, *159*, 104597. [CrossRef]
56. Sanderson, D.J.; Nixon, C.W. The use of topology in fracture network characterization. *J. Struct. Geol.* **2015**, *72*, 55–66. [CrossRef]
57. U.S. Geological Survey. Available online: <https://earthexplorer.usgs.gov/> (accessed on 3 February 2023).
58. Japan Aerospace Exploration Agency. Available online: https://www.eorc.jaxa.jp/ALOS/en/dataset/aw3d30/aw3d30_e.htm (accessed on 3 March 2023).
59. Official Website of Department of Irrigation and Drainage Sarawak. Available online: https://did.sarawak.gov.my/web/subpage/webpage_view/315 (accessed on 15 March 2023).
60. Dowd, P.-I.; Pardo-Iguzquiza, E.; Dowd, P.; Durán Valsero, J.; Robledo, P. A review of fractals in karst. *Int. J. Speleol.* **2019**, *48*, 11–20. [CrossRef]
61. De Carvalho Júnior, O.A.; Guimarães, R.F.; Montgomery, D.R.; Gillespie, A.R.; Gomes, R.A.T.; de Souza Martins, É.; Silva, N.C. Karst depression detection using ASTER, ALOS/PRISM and SRTM-derived digital elevation models in the Bambuí Group, Brazil. *Remote Sens.* **2013**, *6*, 330–351. [CrossRef]

62. Healy, D.; Rizzo, R.E.; Cornwell, D.G.; Farrell, N.J.; Watkins, H.; Timms, N.E.; Gomez-Rivas, E.; Smith, M. FracPaQ: A MATLAB™ toolbox for the quantification of fracture patterns. *J. Struct. Geol.* **2017**, *95*, 1–16. [[CrossRef](#)]
63. Manzocchi, T. The connectivity of two-dimensional networks of spatially correlated fractures. *Water Resour. Res.* **2002**, *38*, 1-1-1-20. [[CrossRef](#)]
64. Haq, B.U.; Hardenbol, J.; Vail, P.R. Chronology of fluctuating sea levels since the Triassic. *Science* **1987**, *235*, 1156–1167. [[CrossRef](#)]
65. Haile, N.S.; Adams, C.G.; Haak, R. *The Geology and Mineral Resources of Suai-Baram Area, North Sarawak*; Brit. Borneo Geol. Mem.; U.S. Government Printing Office: Washington, DC, USA, 1962.

Disclaimer/Publisher’s Note: The statements, opinions and data contained in all publications are solely those of the individual author(s) and contributor(s) and not of MDPI and/or the editor(s). MDPI and/or the editor(s) disclaim responsibility for any injury to people or property resulting from any ideas, methods, instructions or products referred to in the content.